Frequencies and Widths of Phonons in Dilute Cr-W Alloys

K. M. Kesharwani and Bal K. Agrawal
Department of Physics, University of Allahabad, Allahabad-2, India
(Received 14 February 1972)

We have made a detailed study of the effects of force-constant changes on the frequencies and the widths of phonons in random dilute alloys. A nearest-neighbor perturbation model including the changes in the mass and the changes in the central and noncentral force constants has been employed. The theoretical results have been compared with the inelastic neutron scattering experiments recently performed on Cr-W alloys containing different impurity concentrations (0.3, 0.8, 1.6, and 3.0 at.% W). The change in phonon frequency on account of the expansion of the crystal lattice on alloying has been considered to explain the experimental results. Although an over-all good agreement between the low-concentration theory and the experiments has been observed at four different concentrations of tungsten atoms in chromium, there exist some discrepancies in certain frequency regions.

I. INTRODUCTION

It is well known that the study of inelastic-neutron-scattering experiments is the most important tool for the determination of the dispersion relations of all branches of the acoustic- and optical-phonon spectrum in crystals. Elliott and Maradudin[1] discussed a theory of inelastic neutron scattering by lattice vibrations in imperfect crystals and showed the possibility of the detection of the resonance effects by performing coherent neutron scattering experiments. Soon after a number of experiments[2–7] were performed on dilute alloys, such as Cu-Au and Cr-W to observe these effects. In the low-concentration mass-defect theory of Elliott and Maradudin, one assumes that the force constants between the impurity and its neighbors are similar to those of the host lattice and that the perturbation is caused only by the mass change at the impurity site. Almost all the attempts, made on the basis of the mass defect theory to explain the observed shifts and widths of the phonons due to the presence of impurities in the crystal, were found to be inadequate. It was not clear whether the discrepancy between the theory and experiment arises because of the failure of the low-concentration theory which includes only the scattering from a single impurity site and neglects interference effects between the pairs (or the clusters) of the impurities, or whether it arises because of omission of force-constant changes around the impurity atoms.

Any success in accounting for the said discrepancy on the basis of a high-concentration theory was ruled out later by a number of theoretical and experimental investigations. On one hand, Behera and Deo[8] discussed a high-concentration theory based on a graphical method after including the effects of force constant changes in a rather phenomenological way but the situation could not be improved. Hartmann[9] investigated the effects of short-range order within the low-concentration defect theory for a high concentration (9.3 at.%) of gold in copper and observed that the corrections in the resonance region were only of the order of 10%, which were insufficient to remove the discrepancies. On the other hand, the more recent experimental and theoretical investigations of Svensson and Kamitakahara[4] on copper alloys containing low concentrations (1 and 3 at.%) of gold atoms also lead to a similar conclusion. Thus the need for a detailed study of the effects of force-constant changes on the phonons in an imperfect crystal was realized. Some efforts in this direction were made by Lakatos and Krumhansl[10] but they did not consider any experimental result.

In the present paper, we have made a detailed study of the effects of force-constant changes on the phonons of an imperfect crystal and have tried to explain the neutron-scattering experiments performed recently on chromium-tungsten alloys. We observe that the inclusion of the effects of the expansion of the lattice on the phonons on alloying, i.e., the volume effect, is essential to understand the observed phonon shifts especially in the high-frequency region.

The first studies of the effects of impurities using coherent inelastic scattering on Cr–3-at.%-W alloy were carried by Møller and Mackintosh[5] for the $(0, \xi, \xi)T_2$ branch (polarization vector parallel to $[0, \bar{\xi}, \xi]$). Later on these authors extended their measurements for the $(0, \xi, \xi)T_2$ branch and also studied the $(0, 0, \xi)T$ branch in Cr–3-at.%-W alloy.[6] More recently, Cunningham *et al.*[7] have measured the transverse phonon groups in the $(0, 0, \xi)$ and $(0, \xi, \xi)$ symmetry directions in very dilute alloys of chromium containing a number of small concentrations of tungsten (0.3, 0.8, and 1.6 at.% W). In all these attempts, the mass-defect theory has been found to be completely unsuc-

cessful in understanding the observed effects. The discrepancies are not caused by large concentration effects but instead by some other agencies. Thus a more extended perturbation model including the impurity–host-crystal interactions should be considered to understand these experimental results.

We consider here a perturbation model in which changes in the nearest-neighbor central and noncentral force constants of the de Launay type, along with the change in mass, are taken into account. The shifts of the phonon frequencies because of the expansion of the crystal lattice on alloying are calculated by assuming the Grüneisen-mode parameters as variables for the two polarization branches. The calculated frequency shifts are compared with the experimental data for Cr-W alloys containing various impurity concentrations. An over-all good agreement with the experiment is observed except in some frequency regions. The points to be included in the theory for its improvement have also been discussed.

A brief account of inelastic neutron scattering theory for an imperfect crystal has been given in Secs. IIA-IIC. The perturbation model is described in Sec. IID. We describe the lattice dynamics for chromium and the calculation of Green's functions in Secs. IIIA and IIIB, respectively. The effects of force-constant changes due to impurity atoms on the phonons and the lattice expansion effect are discussed in Secs. IIIC and IIID, respectively. The theoretical results are compared with the experiments in Sec. IV. The main approximations taken in the theory are discussed in Sec. V and the main conclusions are included in Sec. VI.

II. THEORY

A. Scattering Cross Section

The scattering of neutrons by lattice vibrations in the Born approximation can be treated in the Fermi-pseudopotential or scattering-length approximation. The problem can be formulated conveniently in terms of the correlation functions or in double-time thermal Green's functions for the atomic displacements. The inelastic, one-phonon cross section for the coherent neutron scattering per unit solid angle per unit interval of outgoing energy per nucleus is given by[1,11,12]

$$\frac{d^2\sigma}{d\Omega\, d\omega} = \frac{|k_2|}{2\pi |k_1|} S_{\rm coh}(\vec{k}, \omega) , \tag{1}$$

where

$$S_{\rm coh}(\vec{k}, \omega) = (A^2/N) \sum_{n,n'} e^{i\vec{k}\cdot|\vec{r}(n)-\vec{r}(n')|} \times \int_{-\infty}^{\infty} dt\, e^{i\omega t} \langle \vec{k}\cdot\vec{u}(n, t)\vec{k}\cdot\vec{u}(n', 0)\rangle , \tag{2}$$

where $\vec{k}_1$ and $\vec{k}_2$ are the incident and the scattered wave vectors of the neutron, respectively, with $\vec{k} = \vec{k}_1 - \vec{k}_2$ and $\hbar\omega = \hbar^2(k_2^2 - k_1^2)/2m$ is the energy transfer to the neutron; m is the mass of the neutron; N is the number of nuclei in the crystal. $\vec{u}(n, t)$ denotes the instantaneous atomic displacement from its equilibrium position $\vec{r}(n)$. The brackets $\langle\ \rangle$ denote a thermal average. A is an average of the effective temperature-dependent scattering length and is defined by

$$A = \langle A_n \rangle = \langle a_n \exp(-\tfrac{1}{2}\langle|\vec{k}\cdot\vec{u}(n)|^2\rangle)\rangle , \tag{3}$$

where the exponential function is the Debye-Waller factor and a_n is the coherent scattering length of the nucleus. The thermalized scattering length A_n is same for every atom in a perfect crystal but may vary from site to site depending on impurity positions in an imperfect solid and leads to incoherent neutron scattering. In general, the impurity usually has a different scattering length than the host atom. Also the Debye-Waller factors for the impurities and their neighbors in the perturbed region are different from that of the host atom. For the coherent scattering, we assume that the thermalized scattering lengths are unaltered in an imperfect crystal, an approximation which is found to be more appropriate at high temperatures. We thus write

$$A_n = a_n e^{-\Lambda} , \tag{4}$$

where $e^{-\Lambda}$ is the Debye-Waller factor for the perfect lattice and is independent of the lattice site n.

The time-dependent correlation functions between the atomic displacements $\langle\vec{u}(n, t)\vec{u}(n', 0)\rangle$ appearing in Eq. (2) may easily be evaluated by the method of Green's functions. The essentially temporal Fourier transform of the correlation function can be written in terms of the Green's function as

$$\int_{-\infty}^{\infty} dt\, e^{i\omega t} \langle u_\alpha(n, t)u_\gamma(n', 0)\rangle = \lim_{\delta\to 0^+} (e^{\beta\omega} - 1)^{-1} [G_{\alpha\gamma}(n, n'; \omega + i\delta) - G_{\alpha\gamma}(n, n'; \omega - i\delta)] , \tag{5}$$

where α, γ denote the Cartesian components of the displacements and $\beta = \hbar/k_B T$. The classical Green's functions $G_\alpha(n, n'; \omega \pm i\delta)$ themselves are the Fourier transforms of the double-time Green's functions, i.e.,

$$G_{\alpha\gamma}(n, n'; \omega \pm i\delta) = (1/2\pi) \int_{-\infty}^{\infty} dt\, e^{i(\omega \pm i\delta)t}\, G_{\alpha\gamma}^{\rm ret\ (adv)}(n, n'; t) . \tag{6}$$

Here the retarded and the advanced Green's functions have been defined as

$$G_{\alpha\gamma}^{\rm ret\,(adv)}(n, n'; t) = \mp 2\pi i\theta(\pm t)\, \langle [u_\alpha(n, t), u_\gamma(n', 0)]\rangle , \tag{7}$$

where the upper (lower) signs stand for the retarded (advanced) Green's function. The brackets [ ] denote the commutator of the operators and the step function $\theta(t)$ is defined by

$$\theta(t)=1 \quad \text{for } t>0$$
$$=0 \quad \text{for } t<0 . \tag{8}$$

If we introduce an impurity substitutionally at a lattice site, the translational symmetry of the host lattice is destroyed and we cannot go over to normal-mode representation. In order to recover the periodicity in the imperfect lattice, we assume that each impurity is equally likely to be at any lattice site and take an ensemble average over all configurations with certain impurity concentration.

Now using Eqs. (2) and (5) and taking the spatial Fourier-transform, we obtain the scattering function for a monatomic crystal as

$$S_{\text{coh}}(\vec{k},\omega)=\frac{A^2}{2\pi N}\frac{1}{(e^{\beta\omega}-1)}\lim_{\delta\to 0}\sum_{s}\sum_{s'}[\vec{k}\cdot\vec{e}(\vec{k}|s)] \times[\vec{k}\cdot\vec{e}(\vec{k}|s')][G_{ss'}(\vec{k},\omega+i\delta)-G_{ss'}(\vec{k},\omega-i\delta)] . \tag{9}$$

Here $\vec{e}(\vec{k}|s)$ are the polarization vectors associated with a plane wave of wave vector $\vec{k}$ in the polarization branch s. The Green's function in the phonon representation has been obtained as

$$G_{ss'}(\vec{k},\omega\pm i\delta)=(1/N)\sum_{nn'}\sum_{\alpha\gamma}[e^{i\vec{k}\cdot\vec{r}_n}e_\alpha(\vec{k}|s) \times G_{\alpha\gamma}(n,n';\omega\pm i\delta)\,e^{-i\vec{k}\cdot\vec{r}_{n'}}e_\gamma(\vec{k}|s)] . \tag{10}$$

Here $\vec{r}_n$, $\vec{r}_{n'}$ denote the lattice vectors of the sites n, n', respectively.

B. Configurationally Averaged Green's Function in the Low-Concentration Limit

The time-independent equation of motion for a pure crystal can be written in the matrix form as[13]

$$\underline{L}_0\vec{\psi}_0=\omega^2\vec{\psi}_0 , \tag{11}$$

where $\underline{L}_0=\underline{M}_0^{-1/2}\underline{\phi}^0\underline{M}_0^{-1/2}$ is the mass-reduced force-constant matrix of the pure lattice, and $\underline{M}_0$ is the mass matrix. $\vec{\psi}_0$ is a vector which is related to the usual atomic displacement vector $\vec{u}$ by

$$\vec{u}=\underline{M}_0^{-1/2}\vec{\psi}_0 . \tag{12}$$

$\underline{L}_0$ is a $3N\times 3N$ matrix for a Bravais lattice.

For a crystal containing a finite concentration of defects which have different masses and interactions with its neighbors than the host atoms, the equation of motion may be written as

$$[\underline{L}_0+\underline{P}(\omega^2)]\vec{\psi}=\omega^2\vec{\psi} , \tag{13}$$

where ω is the frequency of the normal mode and $\underline{P}(\omega^2)$, the perturbation matrix caused by the defects, is explicitly given by

$$\underline{P}(\omega^2)=-\omega^2\underline{M}_0^{-1/2}\Delta\underline{M}\underline{M}_0^{-1/2}+\underline{M}_0^{-1/2}\Delta\underline{\phi}\,\underline{M}_0^{-1/2} . \tag{14}$$

Here the new mass and force constant matrices for the imperfect crystal have been denoted by $(\underline{M}_0+\Delta\underline{M})$ and $(\underline{\phi}^0+\Delta\underline{\phi})$, respectively, and $\vec{\psi}$ is the corresponding vector for the imperfect lattice.

The Green's function for the perturbed crystal is defined by

$$\underline{G}(z)=[\underline{L}_0+\underline{P}(\omega^2)-z\underline{I}]^{-1} , \tag{15}$$

with $\underline{I}$ as an unit matrix and $z=\omega^2+2i\omega\zeta^+$, as the complex squared frequency in the limit $\zeta^+\to 0$. It can also be expressed as

$$\underline{G}(z)=\underline{G}_0(z)-\underline{G}_0(z)\underline{P}(\omega^2)\underline{G}(z) , \tag{16}$$

where the Green's function for the perfect crystal is defined by

$$\underline{G}_0(z)=(\underline{L}_0-z\underline{I})^{-1} . \tag{17}$$

After performing a statistical average over all configurations containing the same number of defects, the configurationally averaged $\{\underline{G}\}$ has the form

$$\{\underline{G}\}=\underline{G}_0-\underline{G}_0\underline{\Sigma}\{\underline{G}\} , \tag{18}$$

where the self-energy $\underline{\Sigma}$ is translationally invariant like $\underline{G}_0$. After going over to the normal-mode representation, the perturbed Green's function is given by

$$\{\underline{G}(\vec{k})\}=\underline{G}^0(\vec{k})-\underline{G}^0(\vec{k})\underline{\Sigma}(\vec{k})\{\underline{G}(\vec{k})\} \tag{19}$$

or

$$\{\underline{G}(\vec{k})\}=[\underline{\omega}^2(\vec{k},s)+\underline{\Sigma}(\vec{k})-z\underline{I}]^{-1} . \tag{20}$$

Thus the real and the imaginary parts of the self-energy $\underline{\Sigma}(k)$ determine the shifts and the widths of the perturbed phonons, respectively.

If we take into account exactly only the scattering of phonons off single impurities and neglect scattering off clusters of impurities, i.e., if we neglect the possibility of neighboring defects interfering with the scattering off a particular defect, the first-order self-energy is given by[14]

$$\underline{\Sigma}_1=c\underline{t}[\underline{I}-c\underline{G}_0\underline{t}]^{-1} , \tag{21}$$

where c is the fractional concentration of defects in the crystal. The $\underline{t}$ is the T matrix for a crystal containing one defect and is given by

$$\underline{t}(z)=\underline{p}(\omega^2)[\underline{I}+\underline{g}(z)\underline{p}(\omega^2)]^{-1} , \tag{22}$$

where the $\underline{p}(\omega^2)$ and $\underline{g}(z)$ are the perturbation and the Green's function matrices which lie in the subspace of a defect ($3b\times 3b$, if b is the total number of atoms directly disturbed by the presence of a single defect including the defect site itself).

For the lowest order in concentration, Eq. (21) may further be approximated by

$$\underline{\Sigma}_1 = c\underline{t} \,. \tag{23}$$

In the above approximation, it has been assumed that the impurities are widely spaced so that one may safely ignore the interference effects between the subspaces of any nearby impurities.

C. Phonon Shifts and Widths

In order to obtain the shifts and the widths of phonons we write the above-obtained self-energy in the normal-mode representation as

$$\underline{\Sigma}(\vec{k}, s) = c \sum_{s'} \langle \vec{k}, s' | \underline{t} | \vec{k}, s \rangle \,. \tag{24}$$

In general, there is a mixing of phonon polarization branches, i.e., for a phonon of a particular polarization s, the phonons are scattered into all the polarization branches. However, in some simple cases such as for a low concentration of defects in the mass-defect model or in the presence of force-constant changes when $\vec{k}$ lies along certain symmetry directions, branch mixing does not occur. In cubic crystals, these symmetry directions are the well known (0, 0, ξ), (0, ξ, ξ) and (ξ, ξ, ξ) directions where $\xi = k/k_{\max}$. Thus, in the presence of trivial nondiagonal terms in $\underline{\Sigma}(\vec{k}, s)$, we may write for one polarization branch

$$\underline{\Sigma}(\vec{k}, s) = \langle \vec{k}, s | \underline{t} | \vec{k}, s \rangle \,. \tag{25}$$

The frequency shifts are, then, given by

$$\omega - \omega_{\vec{k},s} = \Delta\omega = [\mathrm{Re}\underline{\Sigma}(\vec{k}, s)] / (\omega + \omega_{\vec{k},s}) \tag{26a}$$

or

$$\omega - \omega_{\vec{k},s} \simeq [\mathrm{Re}\underline{\Sigma}(\vec{k}, s)] / 2\omega_{\vec{k},s} \tag{26b}$$

in the first approximation.

The phonon full width at half-maximum is given by

$$S = 2[\mathrm{Im}\underline{\Sigma}(\vec{k}, s)] / (\omega + \omega_{\vec{k},s}) \tag{27a}$$

or

$$S \simeq [\mathrm{Im}\underline{\Sigma}(\vec{k}, s)] / \omega_{\vec{k},s} \tag{27b}$$

in the first approximation.

Usually, the dimensions of the perturbation matrix are very large and it is difficult to evaluate the self-energy $\underline{\Sigma}(\vec{k}, s)$. The problem may be simplified immensely if the perturbation has some symmetry. In that case the use of the symmetry coordinates, i.e., the coefficients of the atomic displacements of the symmetrized linear combinations of these in the impurity space block-diagonalizes the matrices $\underline{p}(\omega^2)$ and $\underline{g}(z)$ simultaneously. Let $|\nu, m\rangle$ denote the normalized symmetry coordinate transforming according to the first row of the irreducible representation ν. The index m varies from 1 to m_ν where m_ν is the number of times the irreducible representation ν occurs in $\underline{p}(\omega^2)$. The t-matrix elements may then be written as

$$\langle \vec{k}, s | \underline{t} | \vec{k}, s \rangle = \sum_{\nu, m, m'} l_\nu \langle \vec{k}, s | \nu, m \rangle t_\nu^{mm'} \langle \nu, m' | \vec{k}, s \rangle \,, \tag{28}$$

where l_ν is the degeneracy of the irreducible representation ν, and the contribution of one matrix element of t matrix in the νth irreducible representation is given by

$$t_\nu^{mm'} = \langle \nu, m | \underline{t} | \nu, m' \rangle \,. \tag{29}$$

D. Perturbation Model

Chromium and chromium-tungsten alloys crystallize in bcc structures. We consider the change in mass at the impurity site and the changes in the central and noncentral force constants of de Launay type between the impurity and its nearest neighbors. The matrix $\underline{p}(\omega^2)$ is of dimension 27 $\times$ 27. The substituted impurity possesses O_h point-group symmetry. The irreducible representations occurring in this problem are F_{1u}, F_{2g}, F_{1g}, F_{2u}, E_g, E_u, A_{2u}, and A_{1g}. For details, we refer to an earlier paper[13] by one of the authors, where the results for the t matrix in the various irreducible representations have been obtained for a more general lattice, i.e., for CsCl structure. The expressions are easily applicable to a monatomic lattice where they are further simplified. For the sake of completeness, we reproduce here the expressions for the various irreducible representations of the t matrix. They are as follows:

$$t_{A_{1g}}(z) = \lambda[1 + \lambda(g_1 - 2g_4 + g_5 - 2g_6 - g_7 + 2g_8 - g_9 + 2g_{10})]^{-1} \,, \tag{30a}$$

$$t_{A_{2u}}(z) = \lambda[1 + \lambda(g_1 - 2g_4 + g_5 + 2g_6 + g_7 - 2g_8 + g_9 - 2g_{10})]^{-1} \,, \tag{30b}$$

$$t_{E_u}(z) = \lambda'[1 + \lambda'(g_1 - 2g_4 + g_5 + g_6 + g_7 + g_8 + g_9 - 2g_{10})]^{-1} \,, \tag{30c}$$

$$t_{E_g}(z) = \lambda'[1 + \lambda'(g_1 - 2g_4 + g_5 + g_6 - g_7 - g_8 - g_9 + 2g_{10})]^{-1} \,, \tag{30d}$$

$$t_{F_{2u}}(z) = \lambda'[1 + \lambda'(g_1 - g_5 + g_6 + g_7 + g_8 - g_9)]^{-1} \,, \tag{30e}$$

$$t_{F_{1g}}(z) = \lambda'[1 + \lambda'(g_1 - g_5 + g_6 - g_7 - g_8 + g_9)]^{-1} \,, \tag{30f}$$

$$\underline{t}_{F_{2g}}(z) = \frac{1}{3D_{F_{2g}}(z)} \times \begin{pmatrix} \lambda + 2\lambda' + 3\lambda\lambda' g_{F_{2g}}^{22} & 2(\lambda - \lambda') - 3\lambda\lambda' g_{F_{2g}}^{12} \\ 2(\lambda - \lambda') - 3\lambda\lambda' g_{F_{2g}}^{12} & 2\lambda + \lambda' + 3\lambda\lambda' g_{F_{2g}}^{11} \end{pmatrix}, \tag{30g}$$

where

$$g_{F_{2g}}^{11} = g_1 + 2g_4 + g_5 - g_7 - g_9 - 2g_{10} \,,$$

$$g_{F_{2g}}^{12} = \sqrt{2}(g_6 + g_8) \,,$$

$$g_{F_{2g}}^{22} = g_1 - g_5 - g_6 - g_7 + g_8 + g_9 \,,$$

and

$$D_{F_{2g}}(z)=1+\tfrac{1}{3}[(\lambda+2\lambda')g^{11}_{F_{2g}}+2\sqrt{2}(\lambda-\lambda')g^{12}_{F_{2g}}+(2\lambda+\lambda')g^{22}_{F_{2g}}]+\lambda\lambda'[g^{11}_{F_{2g}}g^{22}_{F_{2g}}-(g^{12}_{F_{2g}})^2]\,. \quad (30h)$$

The optically active F_{1u} mode is given by

$$\underline{t}_{F_{1u}}(z)=\underline{P}_{F_{1u}}(\omega^2)[\underline{I}+\underline{g}_{F_{1u}}(z)\underline{P}_{F_{1u}}(\omega^2)]^{-1}\,, \quad (31a)$$

where

$$\underline{P}_{F_{1u}}(\omega^2)=\frac{1}{3}\begin{pmatrix}-3\epsilon\omega^2+8(\lambda+2\lambda') & -\sqrt{8}(\lambda+2\lambda') & -4(\lambda-\lambda')\\ -\sqrt{8}(\lambda+2\lambda') & (\lambda+2\lambda') & \sqrt{2}(\lambda-\lambda')\\ -4(\lambda-\lambda') & \sqrt{2}(\lambda-\lambda') & (2\lambda+\lambda')\end{pmatrix} \quad (31b)$$

and

$$\underline{g}_{F_{1u}}(z)=\begin{pmatrix}g_1 & \sqrt{8}g_2 & 4g_3\\ \sqrt{8}g_2 & g_1+2g_4+g_5+g_7+g_9+2g_{10} & \sqrt{2}(g_6-g_8)\\ 4g_3 & \sqrt{2}(g_6-g_8) & g_1-g_5-g_6+g_7-g_8-g_9\end{pmatrix}. \quad (31c)$$

Here $\epsilon=(M'-M)/M$ is the mass-change parameter with M' and M as the masses of the impurity and host atom, respectively. The $\lambda(=\Delta\alpha_1)$ and $\lambda'(=\Delta\beta_1)$ are the changes in the mass-reduced, central and noncentral, nearest-neighbor, force constants, respectively, in units of squared frequency. (α_1 and β_1 denote the first-neighbor central and noncentral force constants, respectively). The ten Green's-function matrix elements are given by

$$g_\mu(z)=\frac{1}{N}\sum_{s=1}^{3}\sum_{\vec{k}}\frac{J_\mu(\vec{k}|s)}{\omega^2_{\vec{k},s}-z}\,, \quad (32)$$

where the summation is to be taken over all the wave vectors lying in the first Brillouin zone and $J_\mu(\vec{k}|s)$ for $\mu=1-10$ stands for the following expressions:

$$\begin{aligned}
J_1(\vec{k}|s)&=|e_x(\vec{k}|s)|^2\,,\\
J_2(\vec{k}|s)&=|e_x(\vec{k}|s)|^2\cos(2\pi k_x\tfrac{1}{2}a)\cos(2\pi k_y\tfrac{1}{2}a)\times\cos(2\pi k_z\tfrac{1}{2}a)\,,\\
J_3(\vec{k}|s)&=e_x(\vec{k}|s)\,e_y(\vec{k}|s)\sin(2\pi k_x\tfrac{1}{2}a)\sin(2\pi k_y\tfrac{1}{2}a)\times\cos(2\pi k_z\tfrac{1}{2}a)\,,\\
J_4(\vec{k}|s)&=|e_x(\vec{k}|s)|^2\cos(2\pi k_x a)\cos(2\pi k_y a)\,,\\
J_5(\vec{k}|s)&=|e_x(\vec{k}|s)|^2\cos(2\pi k_y a)\cos(2\pi k_z a)\,,\\
J_6(\vec{k}|s)&=e_x(\vec{k}|s)e_y(\vec{k}|s)\sin(2\pi k_x a)\sin(2\pi k_y a)\,,\\
J_7(\vec{k}|s)&=|e_x(\vec{k}|s)|^2\cos(2\pi k_x a)\cos(2\pi k_y a)\times\cos(2\pi k_z a)\,,\\
J_8(\vec{k}|s)&=e_x(\vec{k}|s)e_y(\vec{k}|s)\sin(2\pi k_x a)\sin(2\pi k_y a)\times\cos(2\pi k_z a)\,,\\
J_9(\vec{k}|s)&=|e_x(\vec{k}|s)|^2\cos(2\pi k_x a)\,,\\
J_{10}(\vec{k}|s)&=|e_x(\vec{k}|s)|^2\cos(2\pi k_y a)\,.
\end{aligned} \quad (33)$$

III. CALCULATIONS AND RESULTS

A. Lattice Dynamics of Chromium

Chromium is a transition metal which shows antiferromagnetic behavior below 313 °K.[15] It crystallizes in a bcc structure with one atom per unit cell. According to Fuchs,[16] the resistance to shear in metals stems usually from two type of interactions (i) the Coulomb interactions between positive ions and negative conduction electrons and (ii) the exchange interaction between the ions assumed to be significant only between the nearest and the next-nearest neighbors. A four-neighbor-force-constant model[17] has been used by Feldman to explain the dispersion curves measured by inelastic-neutron-scattering experiments. This type of calculation does not take into account the influence of free electrons on the lattice dynamical properties of metals. In the present work, we have discussed the lattice dynamics of chromium at room temperature in Kreb's model after considering the first- and second-neighbor ion-ion interactions. In Kreb's model,[18] one considers the effect of electrons on ionic motion through the screening of long-range Coulomb interaction between ions. The values of the elastic constants at room temperature used in the present calculation[15] are $C_{11}=3.500\times10^{12}$ dyn cm^{-2}, $C_{12}=0.678\times10^{12}$ dyn cm^{-2} and $C_{44}=2.008\times10^{12}$ dyn cm^{-2}. The value of the lattice constant is 2.879 18 Å. The values of the effective charge Z and of the Bohm-Pines parameter β are taken to be 1 and 0.353, respectively. We have also considered the factor $f(t)$ appearing in the calculation of the screening parameter k_c. This factor is wave-vector dependent and is given by

$$f(t)=\frac{1}{2}+\frac{1-t^2}{4t}\ln\frac{1+t}{1-t}\,, \quad (34)$$

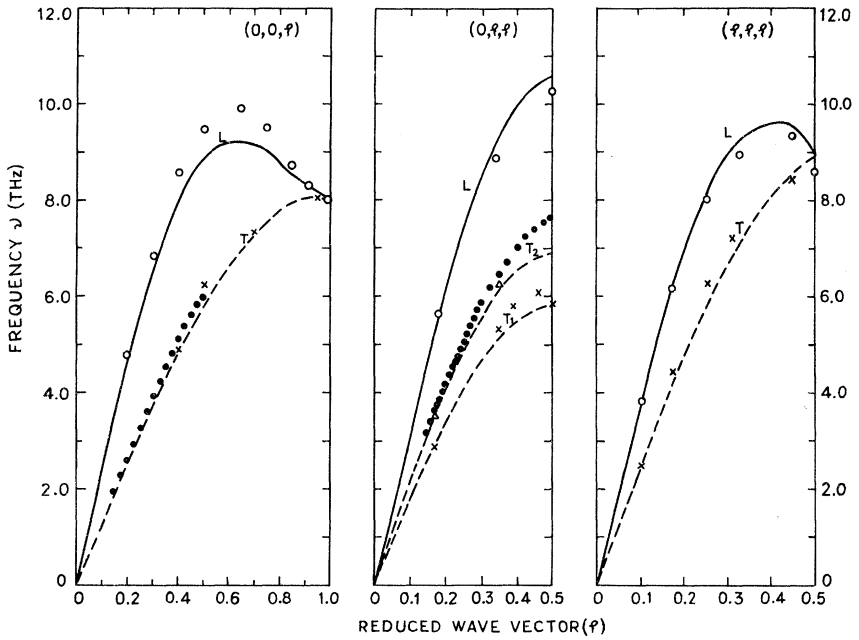

FIG. 1. Dispersion curves for chromium. Experimental data of Møller and Mackintosh (Ref. 19) are marked as ○, ×, and Δ for the longitudinal and the first- and second-transverse branches, respectively. Solid circles represent the measurements of Cunningham *et al.* (Ref. 7).

where $t = k/2k_F$, and k_F is the radius of the Fermi sphere in the wave-vector space.

The eigenfrequencies and eigenvectors were obtained by diagonalizing the dynamical matrix for a bcc lattice of chromium by the Jacobi method. Different mesh sizes were tried and a grid which yielded 8000 points in the Brillouin zone was chosen because it yielded maximum accuracy in reasonable computer time. The results for the three symmetry directions (0, 0, ξ), (0, ξ, ξ), and (ξ, ξ, ξ) have been shown in Fig. 1 ($\xi = k/k_{\max}$). An over-all good agreement is seen with the inelastic-neutron-scattering data of Møller and Mackintosh[19] and Cunningham *et al.*[7] The density of states of chromium has been shown in Fig. 2.

B. Green's Functions

A staggered-bin averaging procedure is followed in the machine computations of the Green's functions given by Eq. (32). The Green's function is separated into real and imaginary parts as

$$g_\mu(\omega^2) = \frac{1}{N}\sum_s \sum_{\vec{k}} \frac{J_\mu(\vec{k}\,|\,s)}{\omega^2_{\vec{k},s} - \omega^2} + i\pi \sum_s \sum_{\vec{k}} J_\mu(\vec{k}\,|\,s)\,\delta(\omega^2_{\vec{k},s} - \omega^2)\,. \quad (35)$$

First the expression $\sum_s \sum_{\vec{k}} J_\mu(\vec{k}\,|\,s)\,\delta(\omega_{\vec{k},s} - \omega)$ is

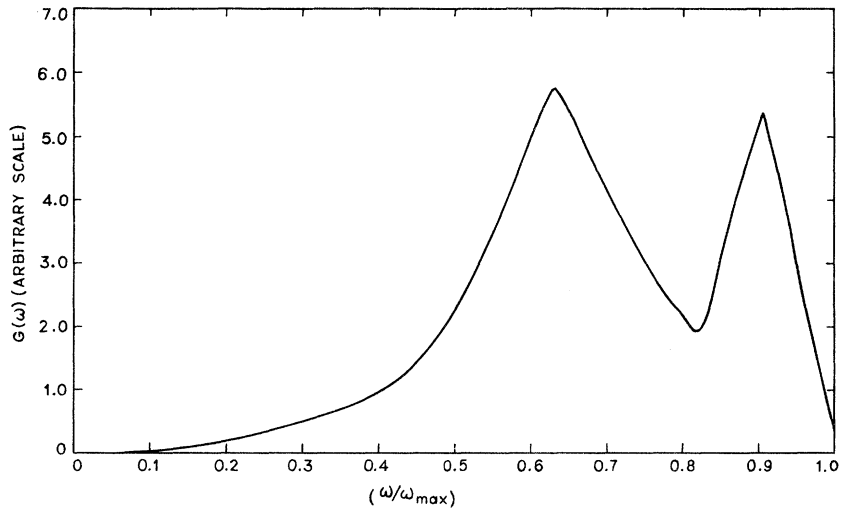

FIG. 2. Frequency spectrum $G(\omega)$ vs ω for chromium.

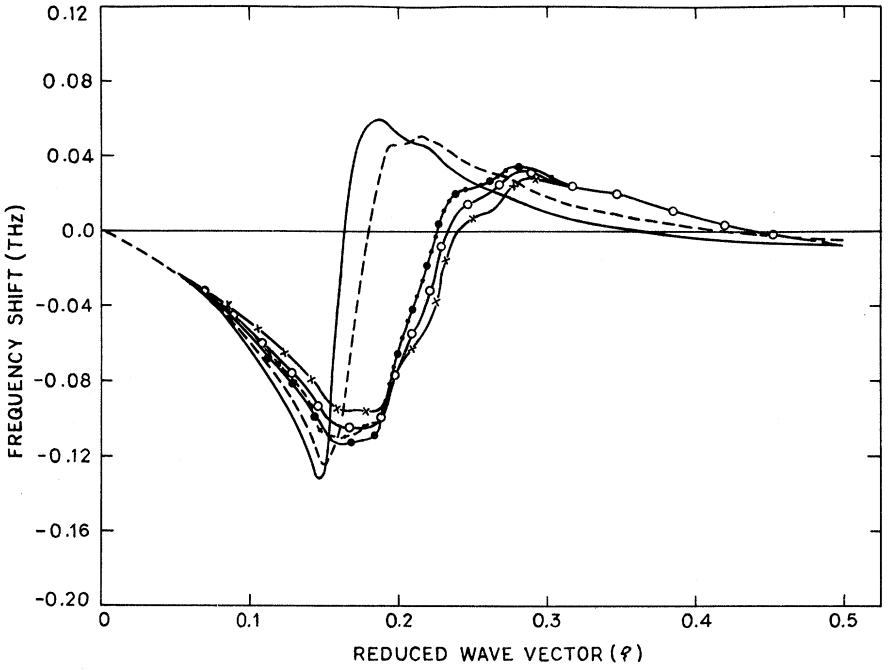

FIG. 3. Comparison of the frequency shifts (no volume effect) for the $(0, \xi, \xi)T_2$ branch plotted against reduced wave vector ξ for the Cr–1.6-at.%-W alloy: (---) mass defect; (—) negative central-force-constant change ($\lambda = -0.12 \times 10^{27}$ sec^{-2}); (-∘-∘-) positive central-force-constant change ($\lambda = 0.55 \times 10^{27}$ sec^{-2}); (-×-×-) positive central- and noncentral-force-constant changes ($\lambda = 0.55 \times 10^{27}$ sec^{-2} and $\lambda' = 0.20 \times 10^{26}$ sec^{-2}); (- - -) positive central- and negative noncentral-force-constant changes ($\lambda = 0.55 \times 10^{27}$ sec^{-2} and $\lambda' = -0.20 \times 10^{26}$ sec^{-2}); (·- ·-) positive central-force constant change ($\lambda = 0.55 \times 10^{27}$ sec^{-2}), calculations made in first approximation. All the other calculations have been made in a self-consistent manner.

calculated and the histograms are obtained for the various Green's functions. To carry out the actual integration for the real part of the Green's functions at low frequencies, the method of Sievers *et al.*[20] has been followed. We may write

$$\mathrm{Re}g_\mu(\omega^2) = \int_0^{\omega_m} d\omega' \, \frac{F(\omega') - F(\omega)}{\omega'^2 - \omega^2} - \frac{F(\omega)}{2\omega} \ln \frac{\omega_m + \omega}{\omega_m - \omega} \quad , \tag{36}$$

where

$$F(\omega) = (1/N) \sum_s \sum_{\vec{k}} J_\mu(\vec{k}|s)\, \delta(\omega_{\vec{k},s} - \omega)$$

and ω_m is the maximum frequency of the lattice. The imaginary part in terms of $F(\omega)$ is given by

$$\mathrm{Im}g_\mu(\omega^2) = (\pi/2\omega) F(\omega) \, . \tag{37}$$

The whole frequency range is divided into 60 equal bins and the histograms are calculated at the center of each bin. Since the mesh points have finite size, the increment in the frequency used in the actual integration should be finite. The value of the increment in the frequency is chosen in such a way that the spurious fluctuations appearing in the Green's functions are minimized. The value 0.25 in the units of the bin width is found to be appropriate in the present calculations.

C. Effects of Force-Constant Changes

It is of much interest to see the difference between the results of the mass-defect theory and those of a theory which includes force-constant changes in between an impurity and its neighbors. The effects of the force-constant changes on the phonon frequencies for the two $(0, \xi, \xi)T_2$ and $(0, 0, \xi)T$ branches have been investigated by varying both the central- and noncentral-force-constant changes. The calculations have been performed for four impurity concentrations, i.e., for 0.3, 0.8, 1.6, and 3.0 at.% W in Cr. As a representative case, we present here some results for 1.6 at.% W in Figs. 3 and 4 for the $(0, \xi, \xi)T_2$ and $(0, 0, \xi)T$ branches, respectively. We find that the force-constant changes greatly influence the frequency shifts especially in the $(0, 0, \xi)$ direction. The qualitative effects of these two parameters λ and λ' are similar but differ in magnitudes. The shifts and widths of the phonons due to noncentral-force-constant changes are seen to be larger in magnitude than those due to central-force-constant changes. A positive force-constant change produces resonance at a higher frequency than that produced by the mass defect, whereas the opposite is the case for negative changes in the force constants. The large negative shifts for phonons just before the resonance frequency can be obtained by using large, negative, force-constant changes but the resonance occurs at the low-frequency side. Large, positive, phonon shifts may be obtained in the high-frequency region only by observing a resonance at a high frequency, but it has the unfortunate effect that the negative shifts greatly decrease in

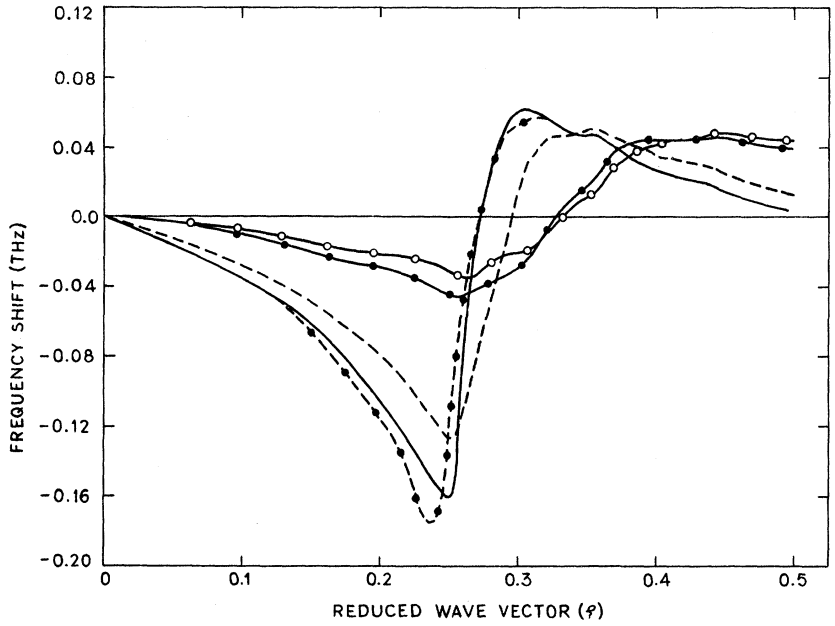

FIG. 4. Comparison of the frequency shifts (no volume effect) for the $(0,0,\xi)$ T branch plotted against reduced wave vector ξ for the Cr–1.6-at.%-W alloy: (---) mass defect; (—) negative central-force-constant change ($\lambda=-0.12\times10^{27}$ sec^{-2}); (-o-o-) positive central-force-constant change ($\lambda=0.55\times10^{27}$ sec^{-2}); (- - -) positive central- and negative noncentral-force-constant changes ($\lambda=0.70\times10^{27}$ sec^{-2}, $\lambda'=-0.40\times10^{26}$ sec^{-2}); (·--·-) positive central-force-constant change ($\lambda=0.55\times10^{27}$ sec^{-2}), calculations made in first approximation. All the other calculations have been made on self-consistent basis.

magnitude prior to the resonance frequency side (a result which is in disagreement with the measured shifts).

We have performed all calculations for the phonon shifts in a self-consistent manner by substituting the frequency modified by defects in the right-hand side of expression (26). In order to see the difference, we have also made computations in the first approximation, i.e., using the unperturbed phonon frequency in the right-hand side of Eq. (26). Some differences are observed in the results obtained in the first approximation and those of a self-consistent one, but they are not very large. The results of a first-approximation calculation have also been included in Figs. 3 and 4.

A comparison of the calculated phonon shifts shown in Figs. 3 and 4 with those of the experi-

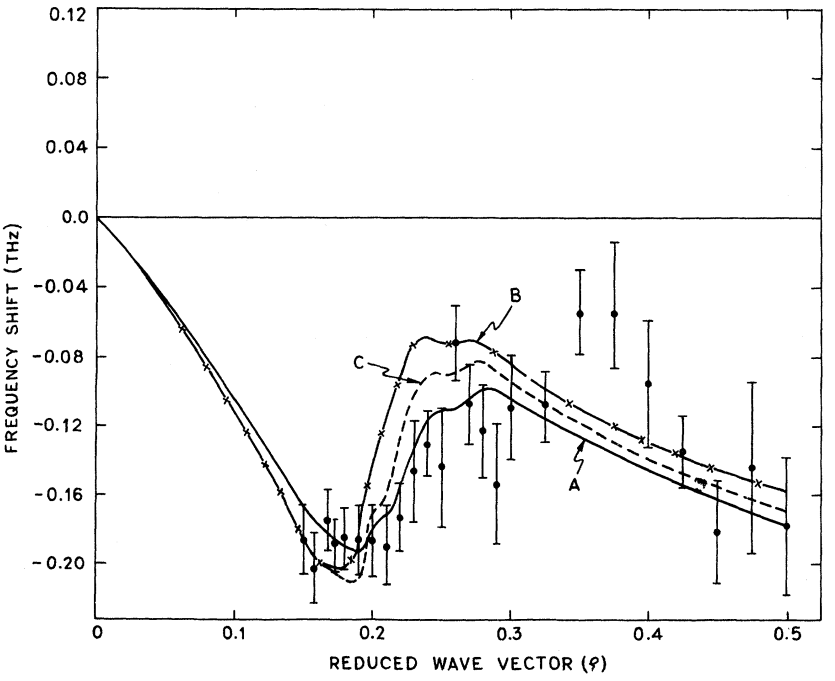

FIG. 5. Calculated frequency shifts in $(0,\xi,\xi)T_2$ branch vs reduced wave vector ξ for Cr–1.6-at.%-W alloy (volume effect included) for different parameters: curve A (—), $\lambda=0.70\times10^{27}$ sec^{-2}, $\lambda'=0.0$, and $\gamma_f=3.5$ sec^{-2}; curve B(-×-×), $\lambda=0.70\times10^{27}$ sec^{-2}, $\lambda'=-0.60\times10^{26}$ sec^{-2} and $\gamma_f=3.0$; curve C(---), $\lambda=0.90\times10^{27}$ sec^{-2}, $\lambda'=-0.60\times10^{26}$ sec^{-2}, and $\gamma_f=3.2$. Solid circles represent the measurements of Cunningham *et al.* (Ref. 7).

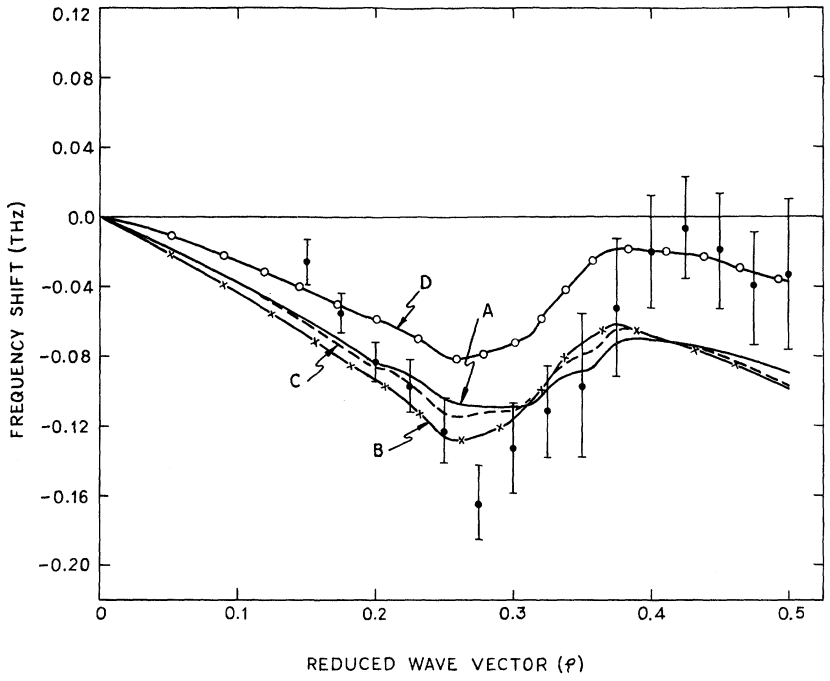

FIG. 6. Calculated frequency shifts in $(0,0,\xi)T$ branch vs reduced wave vector ξ for Cr–1.6-at.%-W (volume effect included) for different parameters: curve A (—), $\lambda = 0.70 \times 10^{27}$ sec^{-2}, $\lambda' = 0.0$ sec^{-2}, and $\gamma_j = 3.5$; curve B(-×-×-), $\lambda = 0.70 \times 10^{27}$ sec^{-2}; $\lambda' = -0.60 \times 10^{26}$ sec^{-2}, $\gamma_j = 3.5$; curve C (----), $\lambda = 0.90 \times 10^{27}$ sec^{-2}, $\lambda' = -0.60 \times 10^{26}$ sec^{-2}, $\gamma_j = 3.5$; curve D (-o-o-), $\lambda = 0.90 \times 10^{27}$ sec^{-2}, $\lambda' = -0.60 \times 10^{26}$ sec^{-2}, $\gamma_j = 2.0$. Solid circles represent the measurements of Cunningham *et al.* (Ref. 7).

mental ones reveals that the calculated positive shifts at high frequencies are not observed experimentally. It suggests the occurrence of some agency which is responsible for an over-all decrease in phonon frequencies. It may be the lattice-expansion effect which will be discussed in Sec. III D.

D. Lattice Expansion Effect

The lattice of pure chromium has been seen to expand when it is doped with tungsten atoms, e.g., for an alloy containing 1.6 at.% W, the percentage change in the lattice parameter is approximately 0.22%. The phonon frequencies are expected to

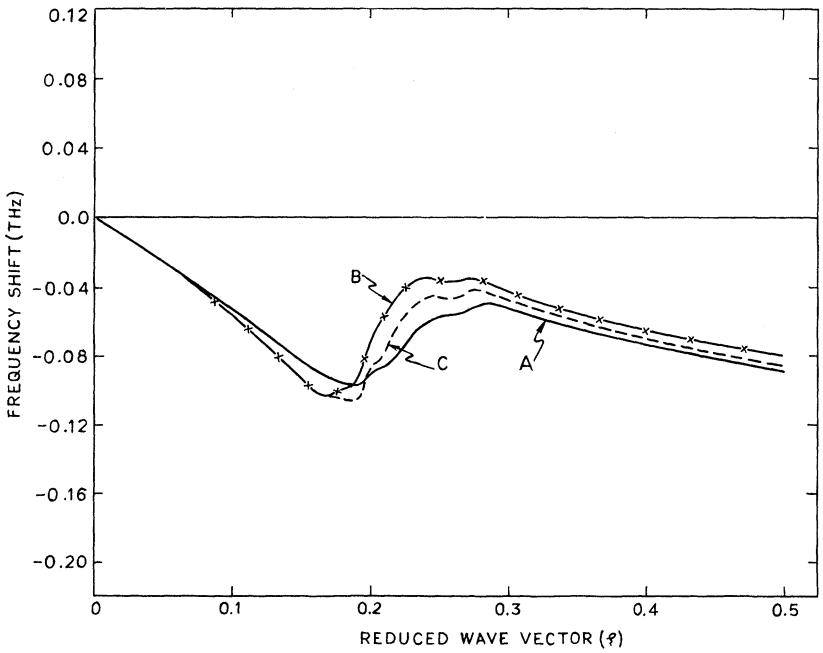

FIG. 7. Calculated frequency shifts in $(0,\xi,\xi)T_2$ branch vs reduced wave vector ξ for Cr–0.8-at.%-W alloy (volume effect included) for different parameters; curve A(—), $\lambda = 0.70 \times 10^{27}$ sec^{-2}, $\lambda' = 0.0$ sec^{-2}, and $\gamma_j = 3.5$; curve B (-×-×-), $\lambda = 0.70 \times 10^{27}$ sec^{-2}, $\lambda' = -0.60 \times 10^{26}$ sec^{-2}, and $\gamma_j = 3.0$; curve C (---), $\lambda = 0.90 \times 10^{27}$ sec^{-2}, $\lambda' = -0.60 \times 10^{26}$, and $\gamma_j = 3.2$.

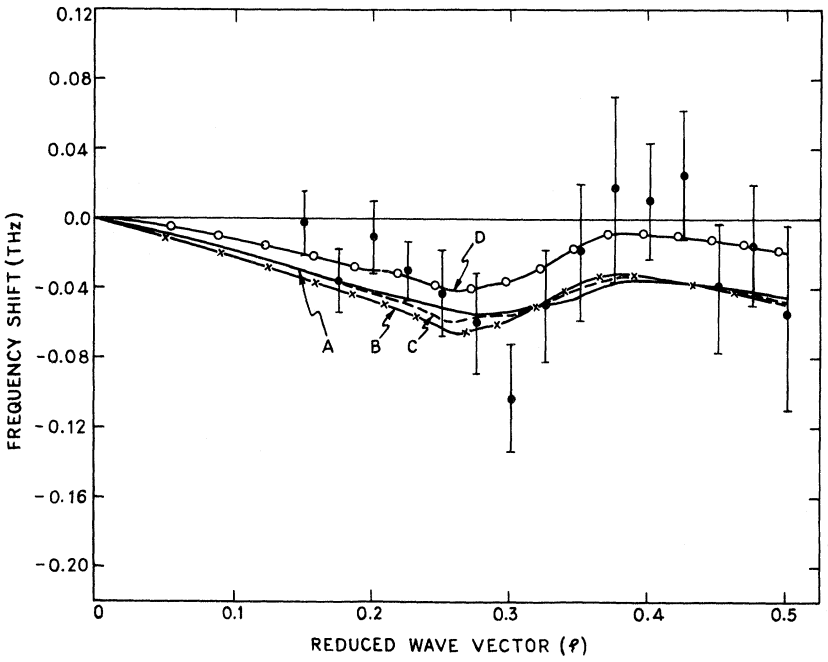

FIG. 8. Calculated frequency shifts in $(0,0,\xi)T$ branch vs reduced wave vector ξ for Cr–0.8-at.%-W alloy (volume effect included) for different parameters: curve A (—), $\lambda = 0.70 \times 10^{27}$ sec^{-2}, $\lambda' = 0.0$ sec^{-2}, and $\gamma_j = 3.5$; curve B (-×-×-), $\lambda = 0.70 \times 10^{27}$ sec^{-2}, $\lambda' = -0.60 \times 10^{26}$ sec^{-2}, and $\gamma_j = 3.5$; curve C (---), $\lambda = 0.90 \times 10^{27}$ sec^{-2}, $\lambda' = -0.60 \times 10^{26}$ sec^{-2}, and $\gamma_j = 3.5$; curve D (-o-o-), $\lambda = 0.90 \times 10^{27}$ sec^{-2}, $\lambda' = -0.60 \times 10^{26}$ sec^{-2} and $\gamma_j = 2.0$. Solid circles represent the measurements of Cunningham *et al.* (Ref. 7).

decrease on account of this expansion. A detailed knowledge of the Grüneisen-mode parameters $(\gamma_j = -\partial \ln \omega_j / \partial \ln V)$ is required to estimate its effects. In general, the mode γ_j varies with the frequency; i.e., it has a structure with respect to the phonon frequency and in order to know it, one should possess a good deal of information about the interatomic potentials in the crystal. One may start by assuming a model potential such as a Morse potential or Rydberg potential and try to study the structure of mode γ's after evaluating the unknown parameters of the potential by utilizing some experimentally measured thermodynamic properties like heat of vacancy formation or isothermal bulk modulus etc. But this type of calculation does not seem to be very reliable. However, the value of the mode γ's for a particular branch in some symmetry direction at $\vec{k} = 0$, i.e., the

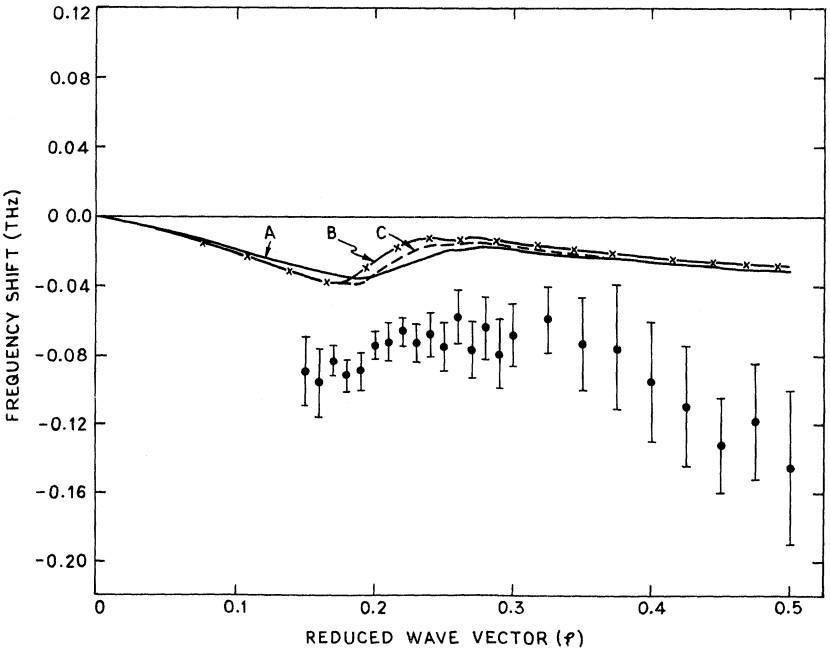

FIG. 9. Calculated frequency shifts in $(0,\xi,\xi)T_2$ branch vs reduced wave vector ξ for Cr–0.3 at.%-W (volume effect included) for different parameters; curve A (—), $\lambda = 0.70 \times 10^{27}$ sec^{-2}, $\lambda' = 0.0$ sec^{-2} and $\gamma_j = 3.5$; curve B (-×-×-), $\lambda = 0.70 \times 10^{27}$ sec^{-2}, $\lambda' = -0.60 \times 10^{26}$ sec^{-2} and $\gamma_j = 3.0$; curve C (---), $\lambda = 0.90 \times 10^{27}$ sec^{-2}, $\lambda' = -0.60 \times 10^{26}$ sec^{-2}, and $\gamma_j = 3.2$. Solid circles represent experimental measurements of Cunningham *et al.* (Ref. 7).

TABLE I. Mass-reduced force constants for pure chromium and their changes due to tungsten at room temperature in units of 10^{26} sec^{-2}.

Force constant	Chromium	Parameters	Changes due to tungsten atom Curve A	Curve B	Curves C and D
α_1[a]	44.91	λ[b]	7.00	7.00	9.00
β_1[c]	0.27	λ'[d]	0.0	−0.60	−0.60
α_2[e]	41.54				

[a]α_1: first-neighbor central force constant.
[b]λ: change in first-neighbor central force constant due to impurity atom.
[c]β_1: first-neighbor noncentral force constant.
[d]λ': change in first-neighbor noncentral force constant due to impurity atom.
[e]α_2: second-neighbor central force constant.

elastic-constant Grüneisen parameter, may be calculated by a knowledge of the pressure derivatives of second-order elastic constants or of the third-order elastic constants. But for chromium metal, no such experimental data are available. In the absence of any reliable information about mode γ's, we resort to the procedure of taking the mode γ's as parameters which remain the same for all frequencies in one symmetry direction for the interpretation of experimental phonon frequency shifts at different impurity concentrations.

IV. COMPARISON WITH EXPERIMENTS

Out of the available experimental data for the four impurity concentrations, i.e., 0.3, 0.8, 1.6, and 3.0 at.% W in chromium, the most suitable set are the Cr–1.6-at.%-W alloy data. More detailed information exists for an alloy containing 3.0 at.% W, in which the phonon widths have also been measured, but the measurements have not been made for $(0, \xi, \xi)T_2$ branch up to the Brillouin-zone boundary. Further, high-concentration effects might be observed in this alloy. The data for Cr–0.8-at.%-W alloy are incomplete because the phonon shifts are available only in the $(0, 0, \xi)$ direction. A better choice would have been the very dilute Cr–0.3-at.%-W alloy but, unfortunately, the results are seen to be in much variation because the experimental errors are comparable with phonon shifts.

The experimental measurements[6,7] for the shifts of the phonon frequencies in the two symmetry directions $(0, \xi, \xi)$ and $(0, 0, \xi)$ have been fitted by varying the two force-constant-change parameters λ and λ' after including the lattice expansion effect. The mode γ is also varied to have best fits. The results for the four different concentrations are presented in Figs. 5–12. In each figure, the results for the three different sets of the perturbation parameters, i.e., for $\lambda = 0.70\times10^{27}$ sec^{-2}, $\lambda' = 0.0$ sec^{-2}; $\lambda = 0.70\times10^{27}$ sec^{-2}, $\lambda' = -0.60\times10^{26}$ sec^{-2}; and $\lambda = 0.90\times10^{27}$ sec^{-2}, $\lambda' = -0.60\times10^{26}$ sec^{-2} are exhibited. The force constants in pure chromium and the fitted force-constant changes in the Cr-W alloys have been shown in Table I. We will now consider each alloy separately.

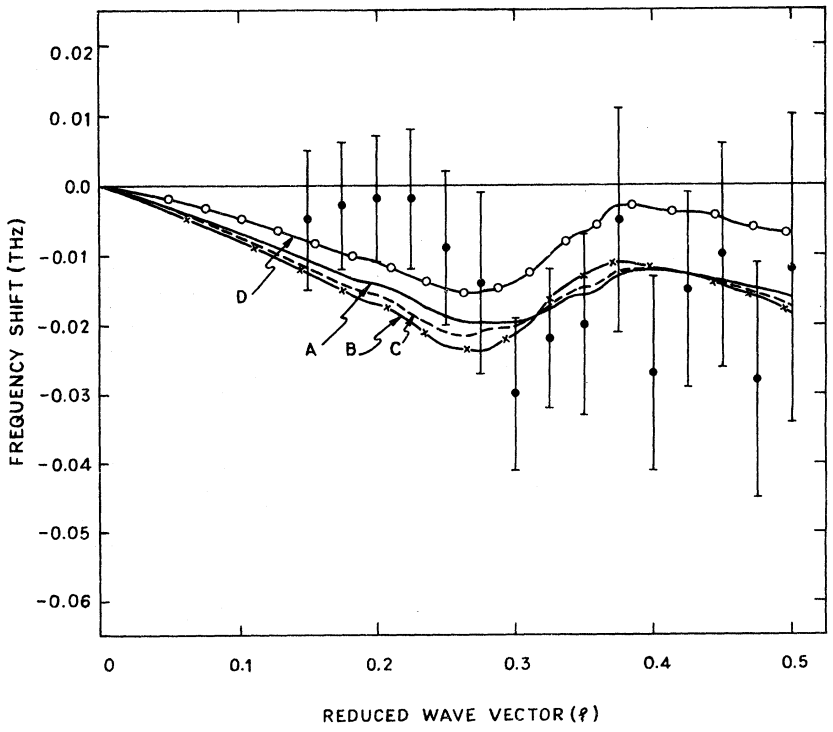

FIG. 10. Calculated frequency shifts in $(0,0,\xi)T$ branch vs reduced wave vector ξ for Cr–0.3-at.%-W alloy (volume effect included) for different parameters; curve A (—), $\lambda = 0.70\times10^{27}$ sec^{-2}, $\lambda' = 0.0$ sec^{-2}, and $\gamma_j = 3.5$; curve B (-×-×-), $\lambda = 0.70\times10^{27}$ sec^{-2}, $\lambda' = -0.60\times10^{26}$ sec^{-2}, and $\gamma_j = 3.5$; curve C(---), $\lambda = 0.90\times10^{27}$ sec^{-2}, $\lambda' = -0.60\times10^{26}$ sec^{-2}, and $\gamma_j = 3.5$; curve D (-o-o-), $\lambda = 0.90\times10^{27}$ sec^{-2}, $\lambda' = -0.60\times10^{26}$ sec^{-2}, and $\gamma_j = 2.0$. Solid circles represent the measurements of Cunningham *et al.* (Ref. 7).

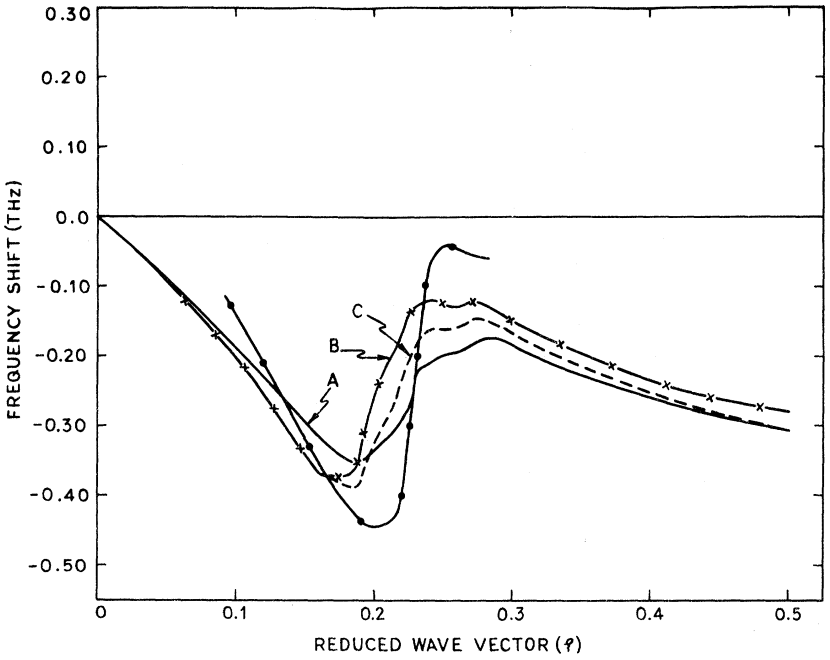

FIG. 11. Calculated frequency shifts in $(0,\xi,\xi)T_2$ branch vs reduced wave vector ξ for Cr–3.0-at.%-W alloy (volume effect included) for different parameters: curve A (—), $\lambda = 0.70\times10^{27}$ sec^{-2}, $\lambda' = 0.0$ sec^{-2}, and $\gamma_j = 3.5$; curve B (-×-×-), $\lambda = 0.70\times10^{27}$ sec^{-2}, $\lambda' = -0.60\times10^{26}$ sec^{-2}, and $\gamma_j = 3.0$; curve C (---), $\lambda = 0.90\times10^{27}$ sec^{-2}, $\lambda' = -0.60\times10^{26}$ sec^{-2}, and $\gamma_j = 3.2$. Curve with solid circles represents the measurements of Mackintosh and Møller (Ref. 6). Experimental errors have not been shown.

A. Cr-1.6-at.%-W Alloy

From Figs. 5 and 6, we note that a high value of γ_j, i.e., 3.5, is seen to be appropriate for obtaining large, negative, frequency shifts in the high-frequency region. We obtain a reasonably good fit in the whole frequency range in the $(0,\xi,\xi)$ direction. The very large negative shifts near the resonance frequency can be obtained by decreasing the noncentral-force-constant change but the agreement becomes worse in the region just above the resonance frequency. An increase in the central force constant does not improve the results as the maximum negative shifts are greatly reduced. From Fig. 6, we observe that in the (0, 0, ξ) direction, there is good agreement with experiment[7] except in the very-high-frequency region where the calculated shifts are seen to be larger.

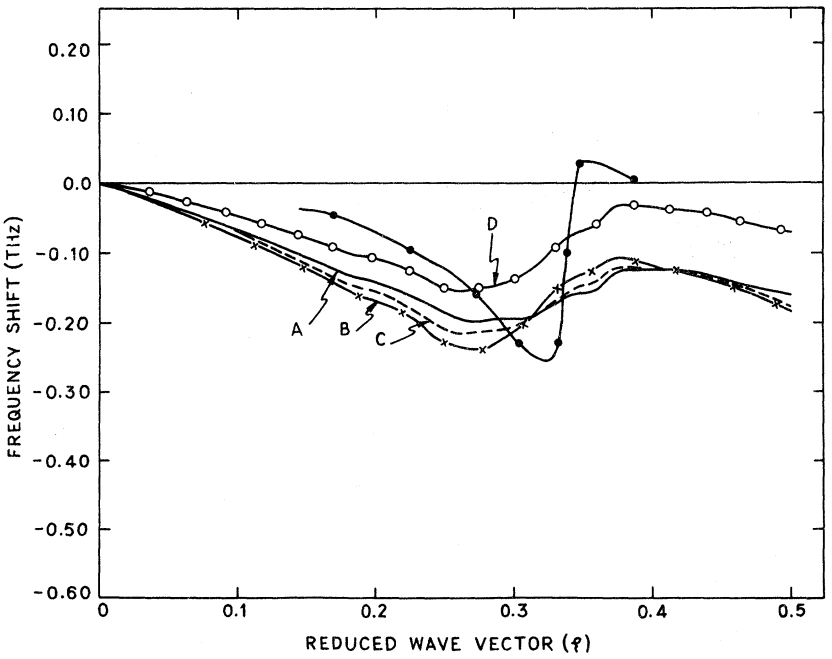

FIG. 12. Calculated frequency shifts in $(0,0,\xi)T$ branch vs reduced wave vector ξ for Cr–3.0-at.%-W alloy (volume effect included) for different parameters: curve A (—), $\lambda = 0.70\times10^{27}$ sec^{-2}, $\lambda' = 0.0$ sec^{-2}, and $\gamma_j = 3.5$; curve B (-×-×-), $\lambda = 0.70\times10^{27}$ sec^{-2}, $\lambda' = -0.60\times10^{26}$ sec^{-2}, and $\gamma_j = 3.5$; curve C (---), $\lambda = 0.90\times10^{27}$ sec^{-2}, $\lambda' = -0.60\times10^{26}$ sec^{-2}, and $\gamma_j = 3.5$; curve D (-o-o-), $\lambda = 0.90\times10^{27}$ sec^{-2}, $\lambda' = 0.60\times10^{26}$ sec^{-2}, and $\gamma_j = 2.0$. The curve with solid circles represents the measurements of Mackintosh and Møller (Ref. 6). Experimental errors have not been shown.

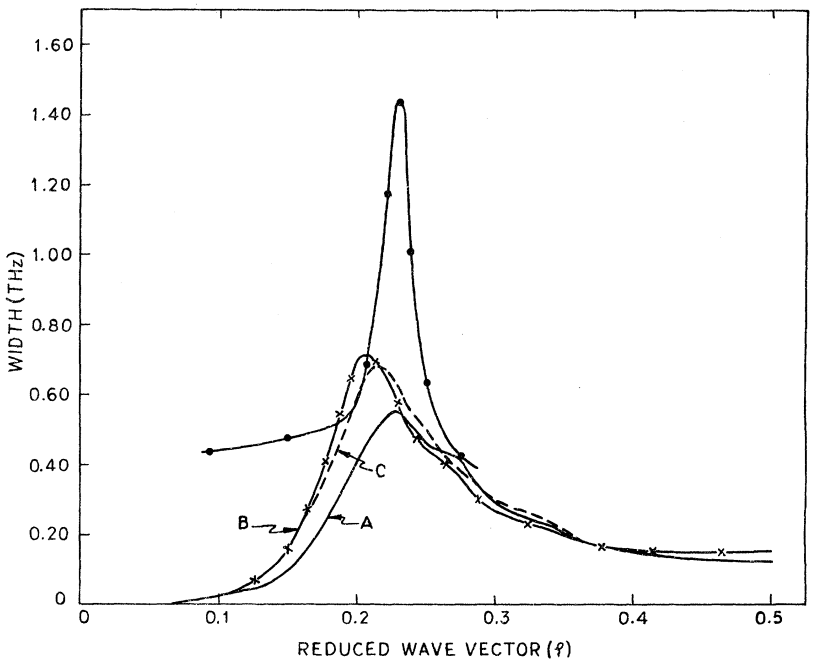

FIG. 13. Calculated phonon widths in $(0, \xi, \xi)T_2$ branch vs reduced wave vector ξ for Cr–3.0-at.%-W alloy (volume effect included) for different parameters: curve A (—), $\lambda = 0.70 \times 10^{27}$ sec^{-2}, $\lambda' = 0.0$ sec^{-2}; curve B (-×-×-), $\lambda = 0.70 \times 10^{27}$ sec^{-2}, $\lambda' = -0.60 \times 10^{26}$ sec^{-2}; curve C (---), $\lambda = 0.90 \times 10^{27}$ sec^{-2}, $\lambda' = -0.60 \times 10^{26}$ sec^{-2}. Curve with solid circles represents the measurements of Mackintosh and Møller (Ref. 6). Experimental errors have not been shown.

The agreement in the high-frequency region could be improved by assuming a small value of γ_j, i.e., $\gamma_j = 2.0$ as shown in Fig. 6, but it greatly reduces the maximum negative shifts.

B. Cr-0.8-at.%-W Alloy

In this alloy, a reasonable agreement of the theory with the experiment[6] is observed in Fig. 8 in the experimentally measured (0, 0, ξ) direction. For completeness, we have also presented the results for the (0, ξ, ξ) direction in Fig. 7. The results in the very-low- and high-frequency regions could be improved by utilizing smaller values of γ_j, but then the large negative shifts are not obtained. The results for $\gamma_j = 2.0$ have also been shown in Fig. 8.

C. Cr-0.3-at.%-W Alloy

The worst disagreement between the theory and the experiment[6] is observed in this very dilute alloy. The measured shifts for Cr–0.3-at.%-W in the $(0, \xi, \xi)T_2$ branch are very large and are difficult to understand (Fig. 9). However, in the (0, 0, ξ)T branch the situation is not so bad. The magnitudes of the calculated shifts are comparable with the experimental ones. The calculated shifts in the low-frequency region are larger than the measured ones whereas they are smaller in the high-frequency regions. A smaller value of $\gamma_j = 2.0$ may improve the situation somewhat in the low-frequency region but it fails miserably in the high-frequency region (Fig. 10).

D. Cr-3.0-at.%-W Alloy

From Figs. 11 and 12 we observe that there is an over-all reasonable agreement between the theory and the experiment[7] but there are discrepancies between the maximum and minimum frequency shifts. A high value of γ_j is favored by the comparison made in $(0, \xi, \xi)T_2$ branch but a lower value of $\gamma_j (= 2.0)$ can be seen to improve the agreement in the low- and high-frequency regions. For this alloy, the phonon widths have also been measured by Møller and Mackintosh.[7] We have calculated the phonon widths and have compared them with the experimental data in Figs. 13 and 14. The widths have also been calculated for other alloys containing different impurity concentrations (0.3, 0.8, and 1.6 at.% W) but as the experimental data are not available, we have not presented the results here. From Figs. 13 and 14, we observe that although the maxima in the phonon width curves appear at the appropriate places, the magnitudes are very small. It seems difficult to obtain such large phonon widths by this theory.

V. DISCUSSION

Although an over-all good agreement with the experiment has been reached discrepancies still exist in certain frequency regions. We should emphasize the main approximations which have been used in the present calculations. Firstly, a nearest-neighbor perturbation model for impurity has been assumed in the present calculations. Since chromium is an antiferromagnetic transition

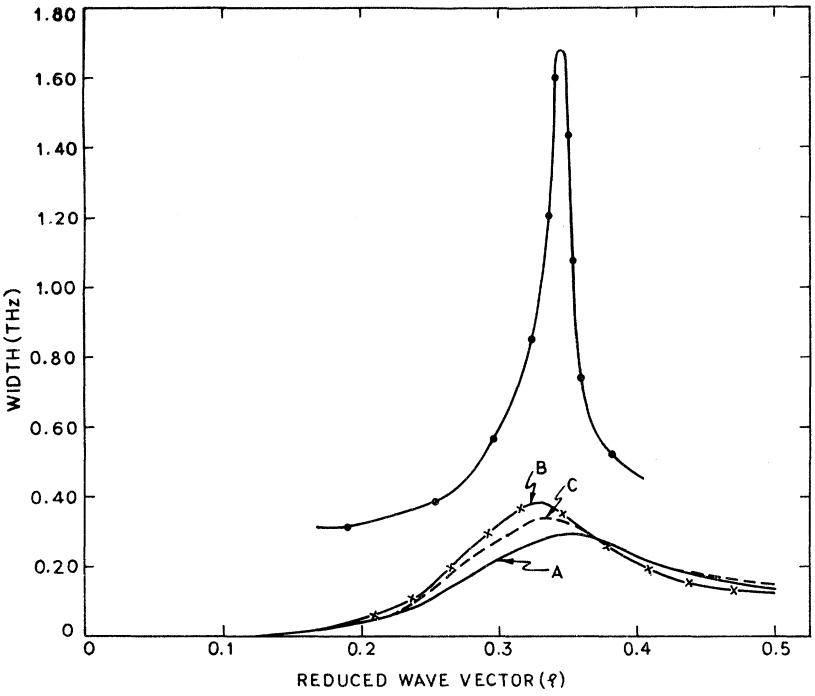

FIG. 14. Calculated phonon widths in $(0,0,\xi)T$ branch vs reduced wave vector ξ for Cr–3.0-at.%-W alloy (volume effect included) for different parameters: curve A (–), $\lambda = 0.70 \times 10^{27}$ sec^{-2}, $\lambda' = 0.0$ sec^{-2}; curve B (-×-×-), $\lambda = 0.70 \times 10^{27}$ sec^{-2}, $\lambda' = -0.60 \times 10^{26}$ sec^{-2}; curve C (---), $\lambda = 0.90 \times 10^{27}$ sec^{-2}, $\lambda' = -0.60 \times 10^{27}$ sec^{-2}. The curve with solid circles represents the measurements of Mackintosh and Møller (Ref. 6). Experimental errors have not been shown.

metal, the exchange interactions between the nearest and next-nearest neighbors are expected to be larger. The replacement of a chromium atom in the host lattice by another transition-metal atom (tungsten) may produce a perturbation which might extend up to second neighbors and even up to more distant neighbors. Thus, there lies a possibility of improvement in the theoretical results by starting with a more extended perturbation model. However, a more important point to be noted is that here one has to work in a situation where no information is available about the mode-Grüneisen parameters. A structure in the mode γ's with respect to phonon frequencies may remove the observed discrepancies in some frequency regions. At present there is no theory which can account well for the lattice expansion effect.

VI. CONCLUSIONS

It has been observed that even small changes in the force constants due to impurity atoms greatly influence the phonon frequencies in crystals. These frequency shifts measured by inelastic neutron scattering experiments can be well understood on the basis of the low-concentration theory after including the effects of the force constant changes plus a correction due to the expansion of the lattice when doped with impurity atoms. High values of the Grüneisen-mode parameters in the two symmetry directions have been found to be essential to understand the measured, large, negative, frequency shifts prior to resonance frequency. However, large discrepancies have been observed in some frequency regions. A detailed knowledge of the structure of mode γ's in the symmetry directions is very much needed to improve the present situation.

ACKNOWLEDGMENTS

The authors are thankful to the Council of Scientific and Industrial Research, India for the financial assistance and to the Delhi School of Economics, Delhi for providing the computation facilities on an IBM 360 computer.

[1]R. J. Elliott and A. A. Maradudin, *Inelastic Scattering of Neutrons* (International Atomic Energy Agency, Vienna, 1965), Vol. I, p. 231.

[2]E. C. Svensson, B. N. Brockhouse, and J. M. Rowe, Solid State Commun. 3, 245 (1965).

[3]E. C. Svensson and B. N. Brockhouse, Phys. Rev. Letters 18, 858 (1967).

[4]E. C. Svensson and W. A. Kamitakahara, Can. J. Phys. 49, 2291 (1971).

[5]H. B. Møller and A. R. Mackintosh, Phys. Rev. Letters 15, 623 (1965).

[6]A. R. Mackintosh and H. B. Møller, *Localized Excitations in Solids* (Plenum, New York, 1968), p. 721.

[7]R. M. Cunningham, L. D. Muhlestein, W. M. Shaw, and C. W. Tompson, Phys. Rev. B 2, 4864 (1970).

[8]S. N. Behera and B. Deo, Phys. Rev. 153, 728 (1967).

[9]W. M. Hartmann, Phys. Rev. 172, 677 (1968).

[10]K. Lakatos and J. A. Krumhansl, Phys. Rev. 180,

729 (1969).
[11]L. S. Kothari and K. S. Singwi, in *Solid State Physics*, Vol. 8, edited by F. Seitz and D. Turnbull (Academic, New York, 1959).
[12]A. Sjolander, in *Phonons and Phonon Interactions, Lectures on Phonons and External Radiation*, 1963 edited by T. A. Bak (Benjamin, New York, 1964).
[13]Bal K. Agrawal, Phys. Rev. 186, 712 (1969).
[14]R. J. Elliott and D. W. Taylor, Proc. Roy. Soc. (London) 296A, 161 (1969).
[15]D. I. Bolef and J. de Klerk, Phys. Rev. 129, 1063 (1963).
[16]K. Fuchs, Proc. Roy. Soc. (London) A153, 622 (1936).
[17]J. L. Feldman, Phys. Rev. B 1, 448 (1970).
[18]K. Krebs, Phys. Rev. 138, A143 (1965).
[19]H. B. Møller and A. R. Mackintosh, *Inelastic Scattering of Neutrons in Solids and Liquids* (International Atomic Energy Agency, Vienna, 1965), Vol. I, p. 95.
[20]A. J. Sievers, A. A. Maradudin, and S. S. Jaswal, Phys. Rev. 138, A272 (1965).
[21]P. W. Sheard, Phil. Mag. 3, 1381 (1958).

PHYSICAL REVIEW B VOLUME 6, NUMBER 6 15 SEPTEMBER 1972

Crystal Dynamics of Lithium Based on the Pseudopotential Technique

Baliram Prasad and R. S. Srivastava
Physics Department, Banaras Hindu University, Varanasi-5, India
(Received 31 January 1972)

The lattice dynamics of bcc lithium have been studied on the basis of a two-parameter model potential proposed by Krasko and Gurskii. A calculation of phonon frequencies, specific heat, and Debye temperature gives a reasonably good agreement with the experimental results.

I. INTRODUCTION

The lattice dynamics of metals have received remarkable theoretical and experimental attention in present years. The neutron diffraction techniques have produced a wealth of data on the vibration spectra of solids, requiring a serious confrontation between theory and experiment. Out of these solids Li, an alkali metal, is the simplest from the theoretical point of view. The ionic size is very small compared with the interionic separations. The conduction electrons can be considered almost free. The Fermi surface is believed on both theoretical and experimental grounds not to be far from spherical. The metal undergoes a Martensitic type[1] of phase transformation into a hexagonal-closed-packed form. This transformation produces a lot of difficulties to the experimental and theoretical investigators. This is one of the reasons for the lack of literature on this metal.

For the first time, Toya[2] calculated the phonon frequencies of Na using the Hartree-Fock method. Dayal and Srivastava[3] made a significant improvement on his results by introducing a slight modification. Several calculations on the pseudopotential approach[4-9] have added considerably to the physical understanding of the crystal dynamics of metals. Recently Wallace[10-12] has calculated the phonon frequencies, binding energies, and Grüneisen parameters for Na, K, and Li using Harrison's modified pseudopotential with considerable success. Gupta and Tripathi[13,14] introduced an exponential term in the Harrison pseudopotential and calculated the phonon frequencies and binding energies with good agreement. Introduction of an exponential term in their potential makes convergence of their series more rapid than those of Wallace. However, these calculations have either given results in slight disagreement with the experiment, or involved extensive fitting of parameters to the measured frequencies. Also these model potentials need an extra exponential term[13-15] to cause the series to converge rapidly.

To overcome these difficulties a model potential was proposed by Krasko and Gurskii,[16] which was used to calculate the crystal stability of some simple metals.[17] It was, therefore, thought worthwhile to treat lithium metal on this model. The values of model parameters are taken from the paper of Gurskii and Krasko.[18] It is seen that our theoretical results are quite reasonable, which confirms the realistic nature of the proposed model potential.

II. GENERAL FORMULATION

The equations of motion for the atoms in a monatomic bcc crystal and the reduction of these equations to a dynamical matrix whose eigenvalues are proportional to the squares of the normal-mode frequencies lead to a 3×3 determinantal equation of the form

$$\left|D_{\alpha\beta}(q) - M\omega^2 I\right| = 0 , \tag{1}$$

where M is the mass of the atom and I is the 3×3 unit matrix. The elements of the dynamical matrix $D_{\alpha\beta}$ are usually represented as a sum of three